External Influences on Hurricane Intensity. Part III: Potential Vorticity Structure

John Molinari, Steven Skubis, and David Vollaro

Department of Atmospheric Science, State University of New York at Albany, Albany, New York

(Manuscript received 8 November 1994, in final form 12 April 1995)

ABSTRACT

The interaction of Hurricane Elena (1985) with a baroclinic wave was reexamined using both potential vorticity (PV) and a formulation for Eliassen–Palm fluxes in cylindrical coordinates. The hurricane began to deepen rapidly as a narrow upper-level positive PV anomaly became nearly superposed over the low-level center. The intensification appeared to represent an evaporation-wind feedback activated by constructive interference of the PV anomalies. Enhanced convection associated with this process eroded the upper PV anomaly and prevented it from crossing the hurricane and reversing the intensification.

The Eliassen–Palm flux divergence showed that maximum eddy activity remained in the upper troposphere prior to the reintensification. This activity was produced in part because the action of the outflow anticyclone of the hurricane contributed to synoptic-scale wave breaking. The upper-level PV anomaly that approached the center was much narrower in extent than the original synoptic-scale trough. The deep layer of vertical wind shear that would have prevented intensification of the hurricane was avoided.

It is concluded that the interaction of a tropical cyclone and a synoptic-scale trough cannot be viewed simply as the bringing together of positive PV anomalies. Rather, the outflow anticyclone, constantly reinforced by the large source of low PV air from the storm core, interacts with and resists shearing by the trough. Whether the hurricane intensifies during such interactions depends to a large extent upon the relative strengths of these positive and negative PV anomalies. Such outflow-layer interactions represent a fruitful area for further research into tropical cyclone intensity change.

1. Introduction

After reaching marginal hurricane strength over the Gulf of Mexico on 29 August 1985, Hurricane Elena changed little in intensity until 2200 UTC 31 August, when it began to deepen rapidly. This deepening occurred when the storm was within 200 km of land and over essentially constant sea surface temperature, hardly conducive conditions for intensification. Molinari and Vollaro (1989a; 1990) provided evidence that interaction of the hurricane with an upper-tropospheric midlatitude trough was responsible for the intensification. By the use of a storm-following cylindrical coordinate, the approach of this trough was shown to produce azimuthal eddy heat and angular momentum sources in the upper troposphere. Nonlinear balanced model solutions showed that upward motion induced by these eddy sources reached the storm core simultaneously with the development of a secondary wind maximum. Rapid deepening of the hurricane was attributed to the contraction of this wind maximum (Willoughby 1990; see also Fig. 9 of Molinari and Vollaro 1990).

The two-dimensional balanced approach provided reasonable insight into the nature of the hurricane intensification as the trough approached. In reality, however, the physical situation most likely does not represent a forcing and response but rather a mutual interaction. Potential vorticity analysis, which has become well established since the major work of Hoskins et al. (1985), provides a powerful tool for investigation of such a process. Potential vorticity (hereafter PV) concepts have been used to describe various processes in idealized tropical cyclones with considerable success (Thorpe 1985; Schubert and Alworth 1987; Shapiro 1992; Montgomery and Farrell 1993; Guinn and Schubert 1993; Ritchie and Holland 1993; McIntyre 1993; Wu and Emanuel 1993, 1994; Möller and Smith 1994). Potential vorticity has only rarely been calculated in real-data hurricane studies. Shapiro and Franklin (1995) have determined the three-dimensional structure of PV in Hurricane Gloria of 1985, including the storm-core region. Bosart and Bartlo (1991) described PV evolution on the synoptic scale during the intensification of Hurricane Diana of 1984. Reilly and Emanuel (1991) and Molinari and Vollaro (1989b) presented brief descriptions of PV in the hurricane environment prior to intensification. In this paper it is proposed to reexamine the interaction of Hurricane Elena (1985) with the upper-tropospheric trough using the PV framework.

Corresponding author address: Dr. John Molinari, Department of Atmospheric Science, Earth Science 225, 1400 Washington Ave., SUNY at Albany, Albany, NY 12222.

The connection between PV and the previous calculations of eddy heat and angular momentum fluxes is provided by Eliassen–Palm (hereafter E–P) fluxes, in that the divergence of the E–P flux is related to the eddy flux of PV. In the current paper, a primitive equation formulation for E–P flux will be derived in a storm-following cylindrical isentropic coordinate. The PV and E–P flux calculations will be used to address two open questions concerning the intensification of Hurricane Elena: (i) the nature of the hurricane interactions with the upper tropospheric PV anomaly that precede the rapid intensification and (ii) the possible mechanisms by which such interactions could bring about the subsequent intensification.

2. Data and analysis methods

All calculations will be made using gridded analyses from the European Centre for Medium-Range Weather Forecasts (ECMWF). These differ from the ECMWF analyses used earlier (Molinari and Vollaro 1990) in that they are uninitialized and have higher resolution in both the horizontal (1.125° latitude–longitude, versus 2.5° earlier) and vertical (12 levels versus 7). The first two factors above do not have significant impact (Molinari et al. 1992), but the added upper-tropospheric levels, especially 150 mb, are needed for adequate PV calculations.

Even the high-resolution analyses have only 50-mb resolution in the upper troposphere and lower stratosphere, and thus the large vertical gradient in PV at the tropopause cannot be fully captured. Detailed horizontal structure of PV near the storm core also cannot be seen by the global analyses. Nevertheless, Elsberry and Kirchoffer (1988) have shown in studies of rapidly intensifying midlatitude storms over open ocean that the ECMWF analyses contain considerable detail in their jet-level PV structure. In addition, Molinari et al. (1992) have shown that ECMWF analyses of hurricanes have quite accurate rotational winds outside of the storm core. This paper will focus upon resolvable scales in the hurricane surroundings and not on PV variation near the core.

Calculations of azimuthal eddy fluxes of various quantities will also be made. Molinari et al. (1992) noted that estimates of such fluxes are remarkably robust in the ECMWF analyses, even though the mean radial velocity (i.e., divergent flow) is not well represented. The reason is that such fluxes usually arise from quasi-balanced synoptic-scale features in the hurricane environment, for which local radial velocity (with respect to the hurricane center) represents mostly rotational flow. The accuracy of all calculations was further aided by the proximity of the United States rawinsonde network during the entire period of study.
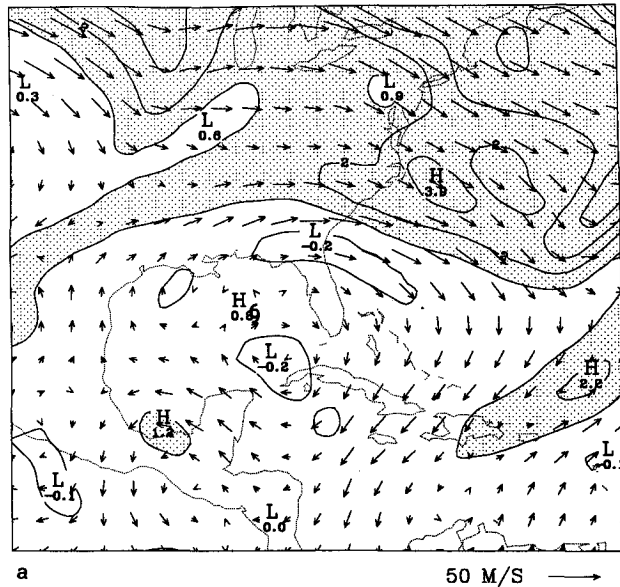

Fig. 1. Wind vectors and Ertel potential vorticity on the 345 K isentropic surface at (a) 0000 UTC 30 August; (b) 1200 UTC 30 August; (c) 0000 UTC 31 August; (d) 1200 UTC 31 August; and (e) 0000 UTC 1 September 1985. The potential vorticity increment is 1 × 10^{-6} m^2 Ks^{-1} kg^{-1} (1 PVU), and values greater than 1 PVU are shaded. Wind vectors are plotted each 2.25° latitude–longitude, one-half their resolution in the gridded analyses. The 345 K surface is at approximately 200 mb in the hurricane environment and ranges from 240–280 mb at the hurricane center. The tropical storm symbol represents the observed position of Hurricane Elena.

3. Potential vorticity evolution

a. Horizontal structure

Hydrostatic Ertel PV is given by

$$\Pi = -g \frac{(\zeta_\theta + f)}{\partial p / \partial \theta}.$$

All fields were linearly interpolated to θ coordinates at 5 K increments, and centered differencing was used for all derivatives. Potential vorticity will be expressed in the units of Hoskins et al. (1985) (1 PVU = 1 × 10^{-6} m^2 K s^{-1} kg^{-1}).

Figures 1a–e show the evolution of Ertel PV on the 345 K surface, beginning about a half-day after the storm initially reached hurricane strength. This surface was chosen for display because it contained the largest eddy activity (see section 4). The 345 K surface lies at approximately 260 mb in the storm core and 180–200 mb over the remainder of the region. In the azimuthally averaged fields the tropopause (defined by the discontinuity in vertical gradient of potential temperature) occurs at 150 mb and about 360 K, so that the 345 K surface lies largely in the upper troposphere not in the lower stratosphere. The same conclusion can be made from Fig. 1 using PV = 1.5 PVU to define the tropopause. Within the 50-mb resolution of the original

b   50 M/S ⟶   c   50 M/S ⟶

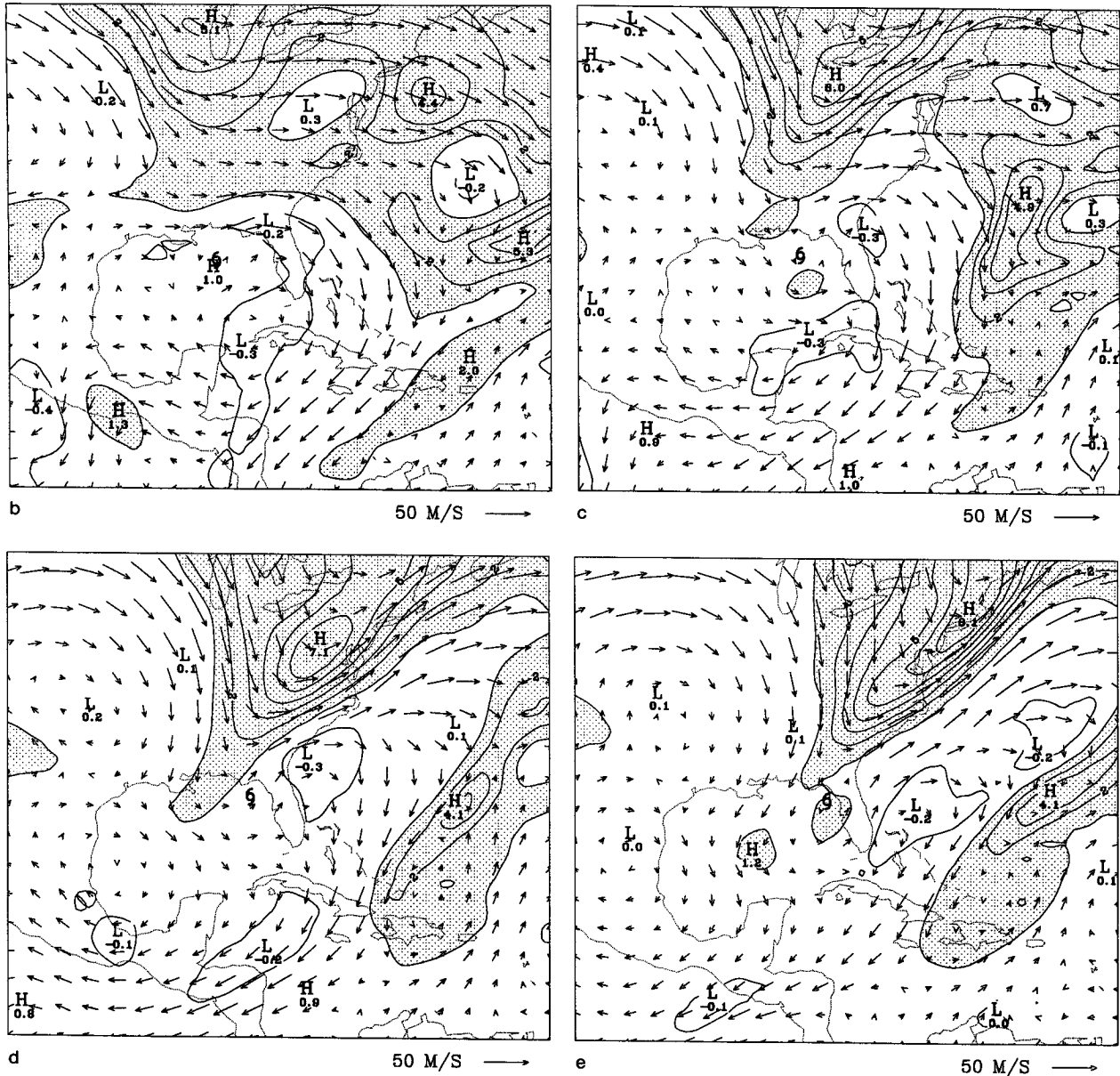d   50 M/S ⟶   e   50 M/S ⟶

FIG. 1. (*Continued*)

analyses, strongest outflow remained at 200 mb throughout the period of study (Molinari and Vollaro 1990). As a result, 345 K remains at or very close to the level of maximum outflow.

The PV at 0000 UTC 30 August (Fig. 1a) shows a well-established outflow anticyclone. A broad region of low-PV air existed around the storm, related, at least in part, to the large supply of near-zero PV air that would be expected to be ejected from the storm at this level (Wu and Emanuel 1993). At this time the trough that eventually interacted with the hurricane was still well to the north-northwest of the center over the central United States.

By 1200 UTC 30 August (Fig. 1b), the midlatitude trough had propagated southeastward to a position directly north of the hurricane. Even at this early time, a wavelike structure in the streamlines had developed around the hurricane, with flow from the west side of the trough passing north of the hurricane and then connecting smoothly with the outflow jet. Twelve hours later (Fig. 1c), the main part of the trough continued eastward, but the base of the trough was retarded in the vicinity of the hurricane. Smaller-scale PV anomalies developed both northwest and northeast of the center. The outflow jet remained almost stationary, so that the wave in the streamlines had a smaller wavelength and

somewhat larger amplitude than previously, indicative of synoptic-scale shearing deformation.

The synoptic-scale deformation of both the trough and the outflow anticyclone continued on 1200 UTC 31 August (Fig. 1d). A narrow positive PV anomaly extended southwestward from the trough about 450 km northwest of the hurricane center. The negative PV anomaly northeast of the center grew in extent. By 0000 UTC 1 September (Fig. 1e), the positive PV anomaly associated with the base of the trough appeared to reach the hurricane center. Part of the strip of PV from the previous time was advected southwestward away from the storm, and the negative PV to the northeast was also apparently advected southeastward. The propagating synoptic-scale trough became even further tilted with respect to the north-south plane as its base stayed in place. The storm had begun to intensify rapidly two hours earlier and continued to do so for nearly 24 hours (Molinari and Vollaro 1989a). The trough did not cross the hurricane center, even at subsequent times.

The PV fields in Fig. 1 resemble what Thorncroft et al. (1993) called an "equatorward Rossby wave breaking." This feature is characterized by anticyclonic shear of the zonal wind south of the maximum westerlies, a southward penetration and lagging of the base of the trough, and a subsequent thinning of the entire trough. The large-scale flow structure favored such a process for several days. The strip of high PV over the southern United States on 0000 UTC 30 August (Fig. 1a) reflected the remains of a previous wave breaking on 27–28 August. The timing and location of wave breaking shown in Figs. 1b–e, however, appeared to be closely associated with the presence of the hurricane outflow layer. In particular, the episode appeared to represent an example of blocking-high-induced wave breaking described by Thorncroft et al., in which the hurricane outflow anticyclone played the role of the blocking high.

Bosart and Bartlo (1991) showed PV evolution in Hurricane Diana of 1984. Some evidence existed for synoptic-scale wave breaking as a mobile trough moved rapidly west to east north of the incipient hurricane (their Figs. 3 and 19). Ultimately only a small PV anomaly approached the storm, while the center of the synoptic-scale trough continued eastward well to the northeast. The initial development of Hurricane Diana thus had some similarities to the reintensification of Hurricane Elena. Because hurricanes frequently encounter mobile upper-tropospheric troughs, this kind of interaction, in which outflow anticyclones contribute to synoptic-scale wave breaking, may represent a common occurrence.

Riehl (1979, p. 482) described the conditions characterizing an upper trough favorable for hurricane intensification: that flow west of the trough axis does not cross the trough but turns anticyclonically and subsides. This is a reasonable description of the process

shown in Fig. 1 and provides further support for the importance of wave breaking in hurricane–trough interactions. The implications of this will be addressed further in the discussion.

b. Vertical structure

Figures 2a–f show the vertical structure of PV in a series of northwest–southeast cross sections through the center of the hurricane at each observation time. The diagram extends from 310 K (about 750 mb near the core) at the bottom to 370 K (130 mb) at the top. The cross sections show the approach of the upper PV anomaly from the northwest and the evolving small horizontal scale of the anomaly during the wave-breaking event. By 1200 UTC 31 August (Fig. 2d) the upper anomaly was about 400–500 km from the center. The increasing vertical wind shear with time is apparent from the southeastward tilt with height of the low-level PV maximum during 31 August. By 0000 UTC 1 September, the upper PV anomaly came very close to the surface center position of the hurricane about the same time as the storm began rapidly intensifying. Twelve hours later (Fig. 2f), as the intensification continued, the PV maximum representing the hurricane was nearly vertical again. The upper PV anomaly had apparently been eroded directly over the storm. The upper anomaly never crossed the hurricane center.

The global analyses from ECMWF cannot, of course, see anything like the true PV at the core, which was likely on the order of 25–50 PVU in this storm (see Shapiro and Franklin 1995). Nevertheless, the detail in the analyses is remarkable, both in the continuity of the PV structure between analysis times and in the seemingly realistic vertical coherence as the analyzed hurricane resisted vertical shear. It is extremely unlikely that ECMWF analyses of hurricanes would always contain such detail (see, for instance, characteristic limitations described by Molinari et al. 1992). The success must arise at least in part because Hurricane Elena was very close to the United States rawinsonde network and because the trough approached from the side with the most data.

The PV evolution in Figs. 1 and 2 represents a synoptic-scale wave breaking followed by partial superposition of the resulting upper PV anomaly and the hurricane. The intensification process implied by the latter geometry will be addressed in the discussion. It will first be noted that the synoptic-scale trough narrowed considerably as it approached the hurricane center as a result of the apparent Rossby wave breaking. This process of wave deformation appears strongly influenced by the hurricane outflow. It can be interpreted in part as an interaction (in the sense of mutual advection) between the hurricane's outflow anticyclone and the synoptic-scale trough. In the following section E–P fluxes in cylindrical coordinates will be examined in order to measure the impact of the resulting wave activity on the hurricane.
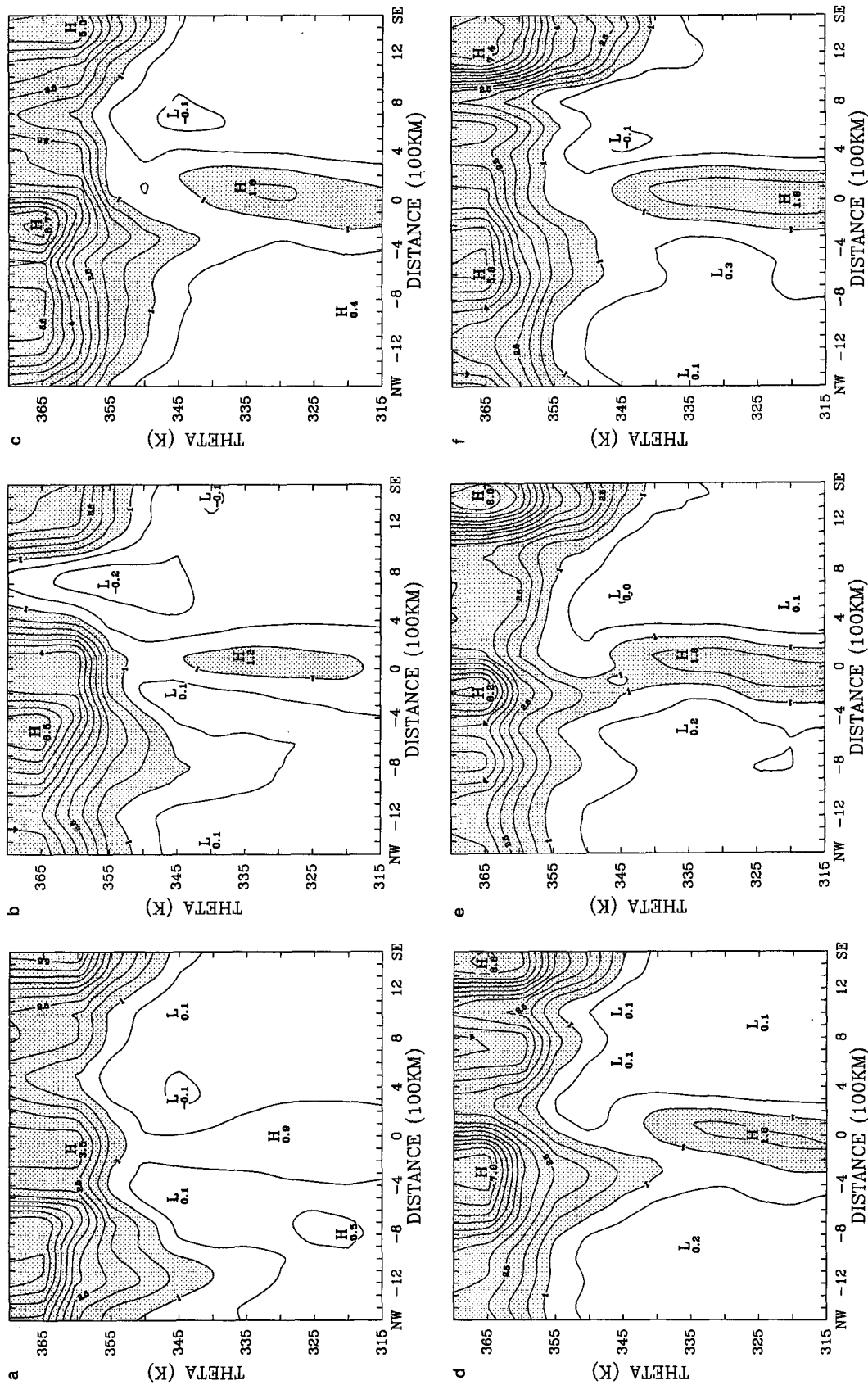
FIG. 2. Cross sections of potential vorticity from northwest (left) to southeast (right) through the observed center of Hurricane Elena for the same times as in Fig. 1, plus (f) 1200 UTC 1 September. Increment: 0.5 PVU.

4. Eliassen–Palm fluxes

a. Equations

The derivation of the E–P flux equations is given in the appendix. It bears some resemblance to that of Schubert (1985) and represents a cylindrical coordinate analog to the spherical coordinate system of Tung (1986). The equations are developed in a storm-following coordinate, which is necessary for producing correct flux terms (Molinari et al. 1993). Like Schubert (1985), analysis has been restricted to θ levels that do not intersect the surface. Because the 300 K level was needed for vertical derivatives at 305 K, and the 295 K surface sometimes went underground due to strong surface heating over the United States southwest, the 305 K level (approximately 850 mb) was the lowest at which the E–P flux was computed.

The equations in the appendix include diabatic heating, friction, and the spatial variation of f. Because the major interactions will be seen to occur in the outflow layer, diabatic heating and friction are likely to be small. It would be difficult to compute heating from global analyses in any event. The terms involving variation of the Coriolis parameter were calculated and found to be small within 900 km of the storm center. As a result, all calculations will be carried out for an adiabatic frictionless f plane. In all equations in the body of the paper, additional small terms that arise from the choice of coordinate (see appendix) will also be neglected. The resulting equation for the time change of pseudodensity-weighted relative angular momentum in a coordinate following the hurricane is given by

$$(r\bar{\sigma}\bar{v}_L)_{t_L} + r^{-1}(r^2(\overline{\sigma u_L})\bar{v}_L)_r + (\overline{r\sigma u})f$$
$$= \nabla \cdot \mathbf{F}_L - (\overline{r\sigma'v'_L})_{t_L}. \quad (1)$$

The subscript L indicates storm-relative flow; all other subscripts represent derivatives. The subscript t_L indicates a time-derivative following the moving storm. Radial and tangential velocity are given by u and v, respectively. Other variables not given below are defined in the appendix. The E–P flux divergence is given by

$$\nabla \cdot \mathbf{F}_L = -r^{-1}(r^2\overline{(\sigma u_L)'v'_L})_r + (\overline{p'\Psi'_\lambda})_\theta,$$

where

$$\mathbf{F}_L \equiv [-r\overline{(\sigma u_L)'v'_L}, \overline{p'\Psi'_\lambda}].$$

The E–P flux vector $\mathbf{F}_L$ can be interpreted as an "effective (angular) momentum flux" (Plumb 1983). The E–P flux divergence represents the impact of both eddy angular momentum fluxes and eddy heat fluxes on azimuthally averaged angular momentum per unit volume $r\bar{\sigma}\bar{v}_L$ [seen by combining the two time derivative terms in (1)]. The radial component of $\mathbf{F}_L$ is the angular momentum flux; the vertical part contains the

heat flux, analogous to a $\overline{T'u'}$ term in pressure coordinates. The relative contribution of each will be shown by plotting $\mathbf{F}_L$ vectors and their divergence in vertical cross sections (Edmon et al. 1980). An outward-pointing arrow represents inward eddy flux of cyclonic angular momentum, and a downward-pointing arrow represents outward eddy heat flux.

The cylindrical coordinate form for E–P flux differs from that commonly used (e.g., Edmon et al. 1980) in that the mean is not a zonal mean but an azimuthal mean that includes the symmetric part of the hurricane. The eddies represent any deviation from the azimuthal mean, including, of course, the midlatitude trough. When $\nabla \cdot \mathbf{F}_L > 0$, eddy activity is producing increasing cyclonic mean angular momentum in the hurricane. Multiplying (1) by $\bar{v}_L$ gives the relevant kinetic energy equation. When $\bar{v}_L < 0$ (anticyclonic mean flow), $\nabla \cdot \mathbf{F}_L > 0$ indicates a mean-to-eddy transfer of energy. In Hurricane Elena this will represent breakdown of the mean outflow anticyclone.

Equation (1) provides an azimuthally averaged rather than local measure of wave activity such as that given by Haynes (1988) and Guinn and Schubert (1993). The above authors also defined a constant basic state. In this study, the basic state is redefined for each observation time because the azimuthal mean evolves between 12-hourly observations and the cylindrical grid itself is moved with the storm. This procedure is necessary to prevent part of the evolving mean from appearing in the eddy effects. It will later be apparent that the eddy activity from the time-varying basic state varies smoothly with time (see also Molinari and Vollaro 1989a, 1990). Although our equation set differs, the purpose of the wave energy flux calculations is similar to that of Guinn and Schubert (1993): to understand the $\bar{v}$ changes associated with PV redistribution.

The relationship between the EP flux divergence and the azimuthal eddy PV flux for frictionless adiabatic flow on an f plane is shown in the appendix [(A14)]. After neglect of two small terms, this is given by

$$-\frac{r\bar{\sigma}^2}{g}\langle u_L^*\Pi_L^*\rangle = \nabla \cdot \mathbf{F}_L - (\overline{r\sigma'v'_L})_{t_L},$$

where the brackets and * indicate pseudodensity-weighted azimuthal mean and deviation, respectively.

The eddy activity, measured either by the E–P flux divergence or the eddy PV flux, can be interpreted as containing two components. The first arises from relative motion between two PV anomalies without change of shape and the second from changes in shape without relative motion. The former could be labeled "superposition" and the latter "interaction." In nature, both are likely to be occurring simultaneously, as the calculations for Hurricane Elena will show.

The E–P flux and its divergence were calculated with the cylindrical grid centered on a rapidly intensi-

fying midlatitude cyclone off the New England coast. The results showed that $\mathbf{F}_L$ vectors were upward at inner radii and turned to outward in the upper troposphere. These results were used as a guide to indicate how a baroclinic development would appear in the cylindrical framework.

b. Results

Figures 3a–e give r-θ cross sections of the EP flux vectors and their divergence for the same times as in Fig. 1. At the initial time (Fig. 3a), the impact of eddy activity as measured by $\nabla \cdot \mathbf{F}_L$ was greatest on the 345 K surface at the radius of the outflow jet. By 1200 UTC 30 August (Fig. 3b), the center of positive E–P flux divergence had significantly increased in magnitude while remaining at 345 K. It was at this time that the wave in the streamlines noted earlier first became prominent. The largest $\nabla \cdot \mathbf{F}_L$ occurred at the 700-km radius, where cyclonic inflow and anticyclonic outflow (with respect to the hurricane center) were largest (Fig. 1b). The EP flux vectors were nearly horizontal within 1000 km of the center, indicating that eddy angular momentum fluxes were playing a much larger role at the level of maximum eddy activity than were eddy heat fluxes.

The center of the synoptic-scale trough moved away from the hurricane over the subsequent 24 hours. As this synoptic-scale feature deformed, the large eddy activity spread over a broad radial range (Fig. 3c). As the base of the upper trough approached the hurricane center at 1200 UTC 31 August (Fig. 3d), the wave activity at the 500-km radius reached its maximum. Throughout the period the E–P flux divergence remained largest at the 345 K level. Weak E–P flux convergence existed at midlevels outside the core. By 0000 UTC 1 September (Fig. 3e), the eddy activity abruptly decreased, consistent with the near superposition of the upper PV anomaly over the hurricane center. The process clearly differs from typical frontal cyclone development, for which the E–P flux vectors would have large vertical components. The downward components of $\mathbf{F}_L$ outside the storm at midlevels reflect the motion of the cold anomaly beneath the trough into the cylindrical volume. Analogous reasoning holds for the upward components in the lower stratosphere.

A physical interpretation for the E–P flux divergence evolution can be seen from the wind and PV fields in Fig. 1. Consider a point at a particular radius on a line of constant azimuth extending from the storm center. If this point lies within a synoptic-scale trough, and if the trough axis through this point contains a clockwise tilt with respect to the intersecting line of constant azimuth, it will import cyclonic eddy angular momentum and export anticyclonic momentum from the cylindrical volume. This interpretation is exactly analogous to that for meridional flux of zonal momentum around a latitude circle. The fact that EP flux vec-

tors are almost entirely horizontal at 345 K allows this barotropic reasoning to be used. An alternative and perhaps more general interpretation from Fig. 1 is that positive PV anomalies are carried inward and negative PV anomalies carried outward with respect to the hurricane center when $\nabla \cdot \mathbf{F}_L > 0$.

Equation (1) is in terms of relative angular momentum, which tends to show substantial impacts at large radii due to its r dependence. It is often preferable to examine the impact of eddy activity on $\bar{v}_L$, which allows physically appealing units of m s^{-1} day^{-1} (Holland 1983; Molinari and Vollaro 1990). For adiabatic frictionless flow on an f plane, the resulting equation (see appendix for details) is given by

$$(\bar{v}_L)_{t_L} + r^{-1}\langle u_L \rangle (r\bar{v}_L)_r + \langle u \rangle f$$

$$= \frac{1}{r\bar{\sigma}} \nabla \cdot \mathbf{F}_L - \frac{1}{\bar{\sigma}} (\overline{\sigma' v_L'})_{t_L} \quad (2a)$$

$$= -\frac{\bar{\sigma}}{g} \langle u_L^* \Pi_L^* \rangle. \quad (2b)$$

In this form of the equation the cross section of E–P flux vectors is no longer useful due to the variable coefficient in front of $\nabla \cdot \mathbf{F}_L$. Instead, a time series of the first right-hand side term in (2a) at 345 K is given in Fig. 4. Analogous to the discussion of (1), the quantity shown in Fig. 4 represents the total effect of eddy activity on $\bar{v}_L$. This quantity was largest at the 500-km radius on 1200 UTC 31 August. The field in Fig. 4 is quite similar to the time series of actual angular momentum flux convergence at 200 mb [see Fig. 5c of Molinari et al. (1992), which corresponds to the ECMWF analyses used here]. This may be the reason that the latter has predictive value for hurricane intensity change even when heat flux effects are omitted (Molinari and Vollaro 1989a; DeMaria et al. 1993).

A time series of azimuthal eddy PV flux at 345 K [right-hand side of (2b)] is shown in Fig. 5. The large inward eddy PV flux on 1200 UTC 31 August is consistent with the movement of the strip of high PV toward the storm center and the resultant PV maximum in the core 12 hours later (Fig. 1e). This field closely resembles the E–P flux divergence term within 1000 km of the center, indicating that the time change term in (2a) is small. In this region, E–P flux divergence is essentially a direct measure of eddy PV flux.

Figures 3–5 show that the large eddy activity associated with the interaction of the outflow anticyclone and the synoptic-scale trough produced a strong inward flux of PV that weakened the mean outflow anticyclone. Figure 6 shows a time series of mean tangential velocity on 345 K. This shows the decay of the mean outflow anticyclone and eventual cyclonic spinup of the storm at inner radii. The large time changes of $\bar{v}_L$ in Fig. 6 correspond reasonably well with large eddy PV flux, although radial advection of absolute momentum by the mean flow [first two left-hand side terms in
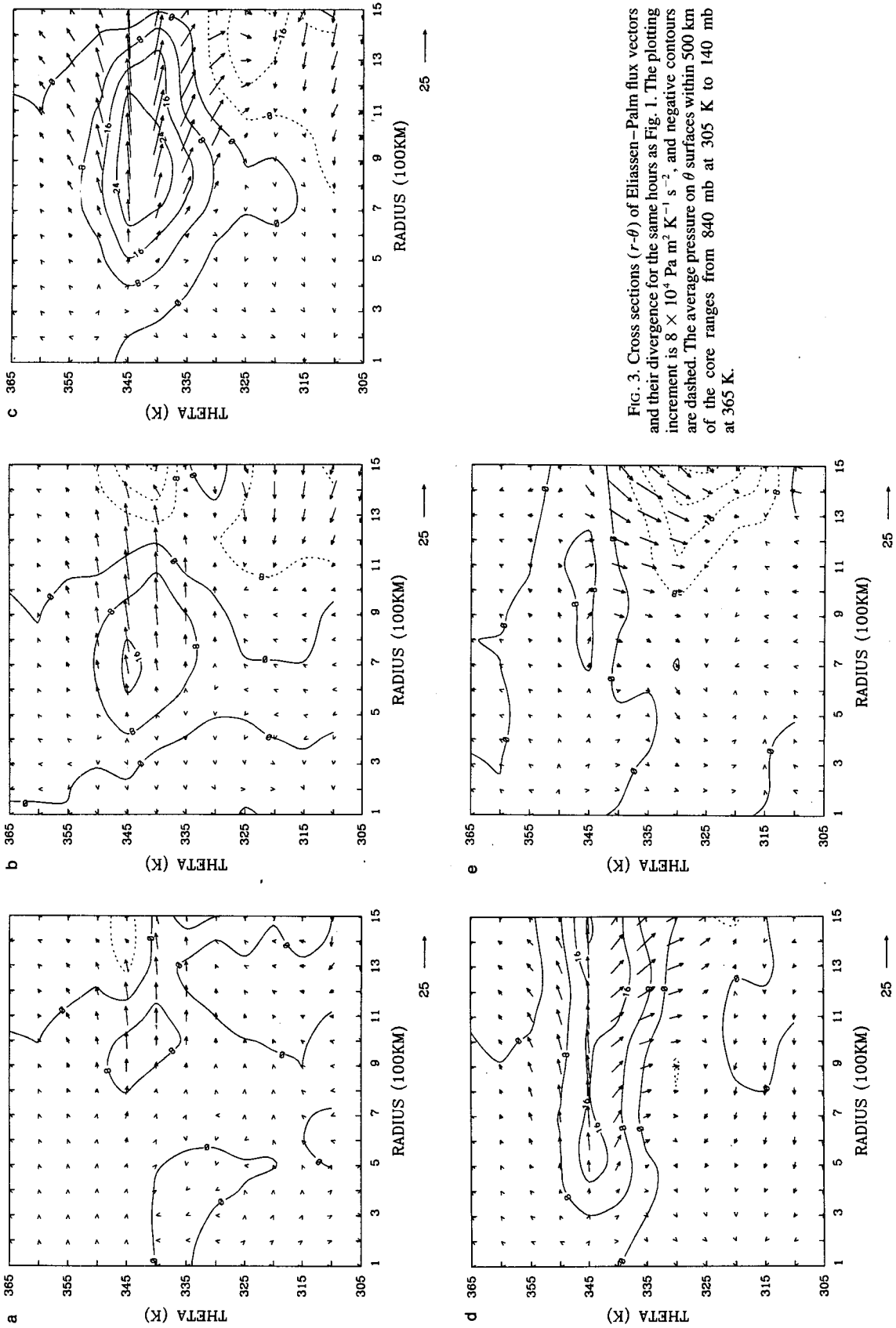
FIG. 3. Cross sections (r-θ) of Eliassen–Palm flux vectors and their divergence for the same hours as Fig. 1. The plotting increment is 8×10^4 Pa m^2 K^{-1} s^{-2}, and negative contours are dashed. The average pressure on θ surfaces within 500 km of the core ranges from 840 mb at 305 K to 140 mb at 365 K.
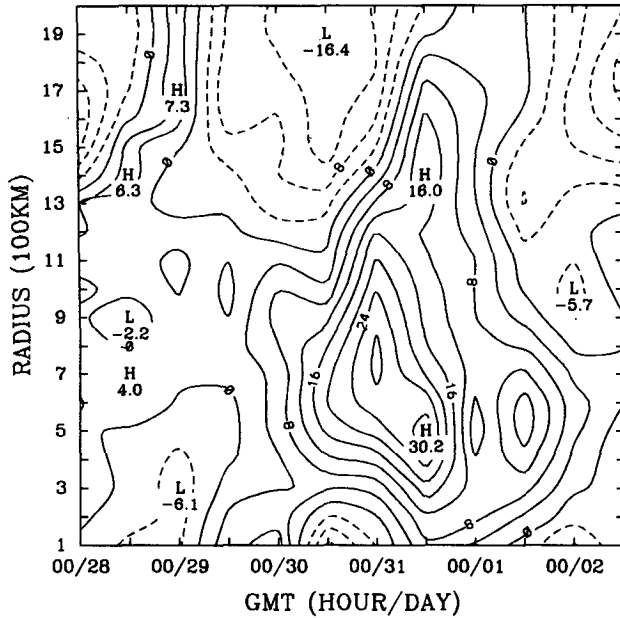
FIG. 4. Radius–time series on the 345 K surface of the impact of wave activity on the mean tangential velocity, given by $(r\bar{\sigma})^{-1}\nabla\cdot F$. The plotting increment is 4 m s^{-1} day^{-1}. Negative contours are dashed.
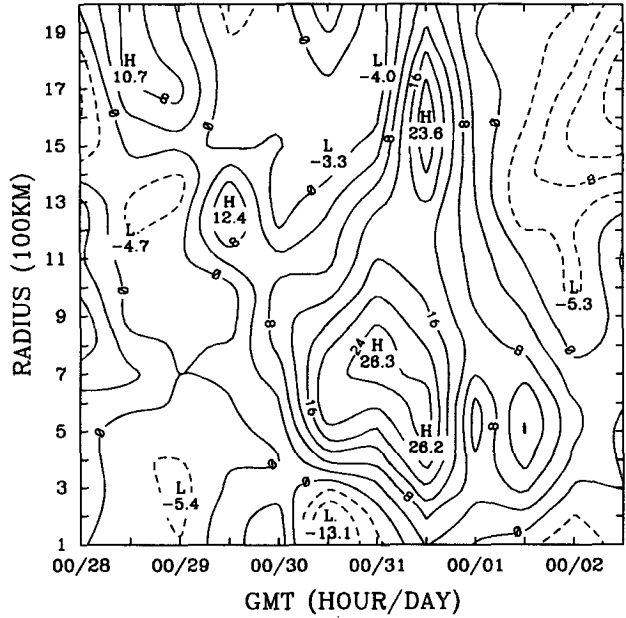

FIG. 5. Radius–time series of time change of tangential velocity brought about by azimuthal eddy flux of potential vorticity, given by $-\bar{\sigma}/g \langle \Pi^* u^* \rangle$. Otherwise as in Fig. 4.

(2a), not displayed] was of comparable magnitude during times of strong outflow. Time series of mean and eddy kinetic energy (also not shown) displayed a large shift from mean to eddy kinetic energy at 345 K between 0000 UTC 30 August and 1200 UTC 31 August.

In summary, the E–P flux cross sections show that large eddy activity remained in the narrow outflow layer throughout the interaction. The eddy activity reflects the integrated influences of the motion of the upper PV anomaly toward the hurricane center, the interaction of the synoptic-scale trough with the outflow anticyclone, and the synoptic-scale Rossby wave breaking. The E–P fluxes by themselves do not give a direct indication of how the storm intensified, in part because these fluxes became small upon the partial superposition of the PV anomalies. The mechanism for intensification will be addressed in the following section.

5. Discussion

a. Importance of the outflow anticyclone

The outcome of an interaction with an upper positive PV anomaly differs fundamentally between tropical cyclones and midlatitude frontal cyclones for two reasons. First, for tropical cyclones, larger ambient vertical shear usually means less intensification (Gray 1968; DeMaria and Kaplan 1994). For midlatitude cyclones, the energy for development comes primarily from the

shear, and rapid intensification requires relatively large vertical shear. Second, tropical cyclones contain an outflow anticyclone (and by implication, large diabatic sources and sinks of PV). When a tropical cyclone is approached by a synoptic-scale trough, it cannot be
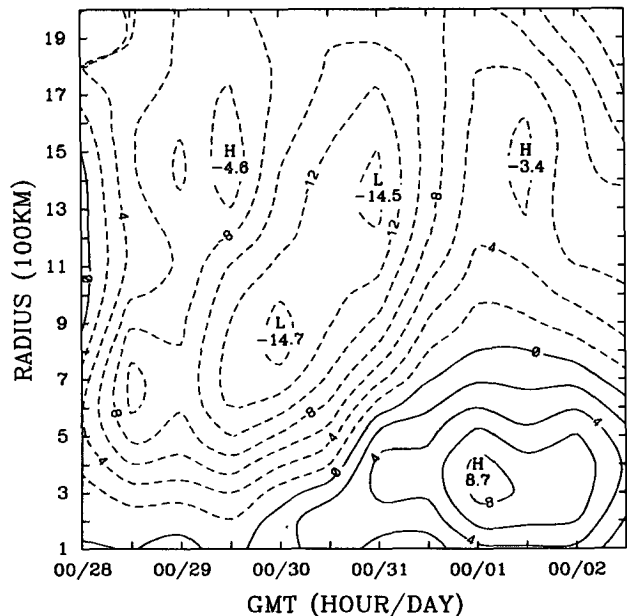

FIG. 6. Radius–time series of azimuthally averaged tangential velocity on 345 K. Plotting increment 2 m s^{-1}.

viewed simply as the bringing together of positive PV anomalies. Rather, the outflow anticyclone, constantly reinforced by the large source of low-PV air from the storm core, interacts with and resists shearing by the trough.

Each of the above factors was important in the reintensification of Hurricane Elena. The breaking synoptic-scale wave was considerably deformed during its interaction with the outflow anticyclone. The upper PV anomaly that ultimately approached the hurricane center was no longer synoptic scale but rather comparable in scale to the hurricane. This process reduced both the vertical penetration depth (Hoskins et al. 1985; Raymond 1992) and the length of time over which substantial vertical wind shear occurred. A deep layer of vertical wind shear might otherwise have prevented intensification of the hurricane. The role of the outflow anticyclone appears to have been critical in modifying the approaching wave to allow for a favorable interaction with the hurricane.

The question is frequently asked in operational hurricane forecasting of how to distinguish between an upper-tropospheric trough that will favorably interact with a tropical cyclone and one that will not. Montgomery and Farrell (1993) argued that the upper PV anomaly had to be strong enough to promote deep sustained ascent, but not so strong as to contain disruptive vertical wind shear. The results of this study support such a view but it is not only the characteristics of the trough that are important. Rather, it is the relative strengths of the positive PV anomaly associated with the trough and the negative PV anomaly associated with the outflow anticyclone that determine the outcome. In a tropical cyclone over warm water with strong core convection, an outflow anticyclone can help to induce synoptic-scale wave breaking, and thus scale reduction, of even a strong trough.

The behavior would be quite different for a tropical cyclone that recently moved over cooler water and lost most of its convection. The synoptic-scale trough could then resist distortion by a hurricane anticyclone no longer reinforced by the convective source of low PV at the center. Unless lower-tropospheric baroclinicity were present to allow extratropical development, the tropical cyclone could be destroyed by the resulting deep layer of vertical shear. This frequently happens to tropical cyclones encountering cool water in the eastern Pacific or at higher latitudes. Over warm water, however, the destruction of a mature tropical cyclone as a result of interaction with an upper-tropospheric trough is extremely unlikely.

b. Mechanism for reintensification of Hurricane Elena

Once the modified upper PV anomaly approached the tropical cyclone core, the exact mechanism for intensification is uncertain. Intensity changes in tropical cyclones are often related to eyewall cycles associated with the development of secondary wind maxima outside the storm core (Willoughby et al. 1982, 1984; Willoughby 1990). Molinari and Vollaro (1990) proposed the following process in Hurricane Elena: (i) nonlinear balanced adjustment of the vortex to the eddy heat and angular momentum sources associated with the upper trough produced enhanced in–up–out circulation; (ii) a secondary wind maximum developed (Willoughby 1990) in response when the forcing reached inner radii; and (iii) this wind maximum contracted as a result of differential adiabatic warming associated with diabatic heating in the presence of a radial gradient of inertial stability (Willoughby 1990; Shapiro and Willoughby 1982). As is typically observed, the storm rapidly intensified as this contracting secondary wind maximum reached the innermost radii. Under these circumstances, understanding the intensification of Elena would reduce to determining how the secondary wind maximum developed. Guinn and Schubert (1993) suggested that outflow-layer asymmetries and their associated circulations could create a mid- or lower-tropospheric PV maximum outside the storm core, either by creating breaking PV waves on the midtropospheric radial PV gradient or by diabatic heating. Ritchie and Holland (1993) and Guinn and Schubert (1993) have shown that filamentation of any such PV maximum in the "surf zone" (McIntyre and Palmer 1984) outside the hurricane core produces a feature much like a secondary wind maximum. Shapiro and Franklin (1995) show an apparent example of such a feature in the PV fields of Hurricane Gloria. These papers thus provide mechanisms by which outflow-layer asymmetries could bring about a secondary wind maximum, as proposed by Molinari and Vollaro (1990).

Alternatively, the development of the secondary wind maximum might not be of central importance. Figure 2 shows that rapid pressure falls began almost simultaneously with the near superposition of the upper and lower PV anomalies. Reintensification may represent "constructive interference without phase locking" (Emanuel, personal communication, 1988; Hoskins 1990, 68–69; Farrell 1985). By this reasoning, as the PV anomalies come within a Rossby radius, the pressure and wind perturbations associated with the combined anomalies are greater than when the anomalies are apart, even though the PV magnitudes are unchanged. The perturbation energy comes from the basic-state shear that brought the anomalies together. This argument is based on quasigeostrophic reasoning but can be extended qualitatively to higher-order balances (Emanuel, personal communication, 1988). A quantitative estimate of such perturbations could be made in this case only by using the PV inversion techniques of Davis and Emanuel (1991) and Davis (1992).

Constructive interference without some additional diabatic component cannot account for the observed intensification because (i) the Eliassen–Palm fluxes

showed little evidence of baroclinic development and (ii) Figs. 1 and 2 show that the upper PV anomaly never crossed the storm and thus never reversed the intensification process. The latter behavior resembles that in the idealized balanced model integrations of tropical cyclogenesis in response to upper-tropospheric PV anomalies by Montgomery and Farrell (1993). Their "dry" integration behaved like pure constructive interference, with small deepening of the lower PV anomaly that was quickly reversed. In their "moist" integration with diabatic heating (simulated by changing the effective static stability), deep ascent occurred and the tropical cyclone intensified by stretching at lower levels. The upper anomaly was rapidly eroded by heating in the latter integrations, qualitatively similar to what was seen in Hurricane Elena.

Montgomery and Farrell (1993) did not explicitly include surface fluxes. Emanuel et al. (1994) have emphasized the potentially misleading nature of interpreting tropical circulations as driven by latent heating. Following their reasoning, it is proposed that the reintensification of Hurricane Elena represented a baroclinic initiation of the wind-induced surface heat exchange mechanism (WISHE; Emanuel 1986; Rotunno and Emanuel 1987; Emanuel et al. 1994). By this mechanism, the constructive interference induces stronger surface wind anomalies, which produce larger surface moisture fluxes and thus higher surface moist enthalpy. This feeds back through the associated convective heating to produce stronger radial–vertical circulations and thus stronger surface winds. The effects of the enhanced convective heating on the upper anomaly would be as described above. The small effective static stability in the saturated, nearly moist neutral storm core ensures a deep response so that even the rather narrow upper trough can initiate the WISHE process. The key to this mechanism is the direct influence of the constructive interference on the surface wind field.

Available data cannot confirm this speculation as to what occurs at the hurricane core, nor can it determine the possible role of the secondary wind maximum. This would require detailed knowledge of the three-dimensional structure and evolution of PV in the hurricane. Shapiro and Franklin (1995) have shown this is a daunting task, even in a storm with extensive inner-core data. No definitive conclusion can be made as to whether the secondary wind maximum was an essential or incidental part of the above process.

Idealized numerical models provide an alternative. A simple shallow water model containing a simulated outflow anticyclone (Ooyama 1987; Wu and Emanuel 1993) could be combined in the initial state with a propagating Rossby wave train to examine outflow-layer interactions. A more complex model would be required to simulate three-dimensional aspects, especially the influence of diabatic heating. Such a model must cover a wide enough region to describe synoptic-

scale motions, yet have enough resolution to simulate the hurricane core and secondary eyewall cycles. Computer power may just be developing to the point where such a simulation is feasible.

6. Conclusions

Potential vorticity is a powerful tool for simplifying the dynamical interpretation of interacting disturbances. Evidence has been provided that the reintensification of Hurricane Elena began during partial superposition of an upper-tropospheric positive potential vorticity anomaly over the hurricane. It is proposed that this superposition initiated the evaporation–wind feedback instability (WISHE) of Emanuel (1986).

An essential part of the evolution occurred prior to the superposition during the interaction of the outflow anticyclone with the approaching trough. The associated synoptic-scale wave breaking thinned the trough, effectively reducing the duration and penetration depth of the accompanying vertical wind shear. This prevented dramatic weakening of the storm as the upper PV anomaly approached. It is proposed that the interaction between upper-tropospheric positive and negative PV anomalies has not been sufficiently studied and is a fruitful area for further research into tropical cyclone intensity change.

APPENDIX

Eliassen–Palm Flux in Cylindrical Coordinates

a. Fixed spatial coordinate

The relative angular momentum equation for hydrostatic flow with θ as a vertical coordinate is given by (derivatives are indicated by subscripts)

$$(rv)_t + u(rv)_r + vr^{-1}(rv)_\lambda + \dot{\theta}(rv)_\theta$$

$$= -(\Psi)_\lambda - rfu + rF^\lambda, \quad (A1)$$

where u and v are radial and tangential velocity, respectively, F^λ is the azimuthal component of frictional force per unit mass, Ψ is Montgomery streamfunction, and other terms have their usual meaning. The equation of mass continuity for hydrostatic flow in isentropic coordinates is

$$\sigma_t + r^{-1}(r\sigma u)_r + r^{-1}(\sigma v)_\lambda + (\sigma\dot{\theta})_\theta = 0, \quad (A2)$$

where $\sigma \equiv -p_\theta$ is the pseudodensity. Combining (1) and (2) gives the flux form of the equation for relative angular momentum weighted by pseudodensity:

$$(\sigma r v)_t + r^{-1}(r^2 \sigma u v)_r + r^{-1}(r \sigma v^2)_\lambda$$
$$+ (r \sigma v \dot\theta)_\theta = -\sigma \Psi_\lambda - r \sigma f u + r \sigma F^\lambda. \quad (A3)$$

The variables u, v, $\dot\theta$, and f are divided into azimuthal mean and eddy components, where

$$(\bar\alpha) \equiv \frac{1}{2\pi} \int_0^{2\pi} \alpha \, d\lambda; \quad (\alpha)' = (\alpha) - (\bar\alpha).$$

After azimuthally averaging, (3) becomes

$$(r\bar\sigma\bar v)_t + r^{-1}(r^2(\overline{\sigma u})\bar v)_r + (r(\overline{\sigma\dot\theta})\bar v)_\theta + r(\overline{\sigma u})\bar f$$
$$= \nabla \cdot \mathbf{F} - (r\overline{(\sigma\dot\theta)'v'})_\theta - (r\overline{\sigma'v'})_t$$
$$- r\overline{(\sigma u)'f'} + r\bar\sigma\overline{F^\lambda}, \quad (A4)$$

where the E–P flux divergence is given by

$$\nabla \cdot \mathbf{F} = -r^{-1}(r^2\overline{(\sigma u)'v'})_r + (\overline{p'\Psi_\lambda'})_\theta,$$

and

$$\mathbf{F} \equiv [-r\overline{(\sigma u)'v'}, \overline{p'\Psi_\lambda'}]$$

is the E–P flux vector. For adiabatic frictionless motion on an f-plane, (4) is equivalent to the expression of Schubert (1985). The full expression (4) represents a cylindrical analogue to Tung's (1986) spherical coordinate version [his (2.86)]. The first three right-hand side terms in (4) constitute the cylindrical version of Tung's (1986) pseudo E–P flux divergence.

Tung (1986) showed that the pseudo E–P flux divergence can be related to an eddy PV flux. In cylindrical coordinates, the eddy PV flux form for the rhs of (4) can be obtained by substituting the azimuthal means of (1) and (2) into the rhs of

$$(r\bar\sigma\bar v)_t = (\bar\sigma)_t r\bar v + \bar\sigma(r\bar v)_t. \quad (A5)$$

After some algebra, this yields an eddy PV flux expression

$$(r\bar\sigma\bar v)_t + r^{-1}(r^2(\overline{\sigma u})\bar v)_r + (r(\overline{\sigma\dot\theta})\bar v)_\theta + (r\overline{\sigma u})\bar f$$
$$= -\frac{r\bar\sigma^2}{g}\langle u^*\Pi^*\rangle - r\bar\sigma(\bar\theta^* v_\theta) + r\bar\sigma\overline{F^\lambda}, \quad (A6)$$

where

$$\langle\alpha\rangle \equiv \frac{(\overline{\sigma\alpha})}{\bar\sigma}$$

$$(\alpha)^* \equiv (\alpha) - \langle\alpha\rangle = (\alpha)' - \frac{(\overline{\sigma'\alpha'})}{\bar\sigma}$$

are respectively defined as the pseudodensity-weighted azimuthal mean and deviation, and the hydrostatic Ertel potential vorticity (PV) is defined as

$$\Pi \equiv g\frac{(\zeta_\theta + f)}{\sigma},$$

where

$$\zeta_\theta = r^{-1}(rv)_r - r^{-1}u_\lambda$$

is the relative vorticity on a θ surface. The pseudodensity-weighted flux of pseudodensity-weighted PV can be written in terms of a more traditional azimuthal eddy flux plus two higher-order terms:

$$\frac{r\bar\sigma^2}{g}\langle u^*\Pi^*\rangle = \frac{r\bar\sigma^2}{g}(\overline{u'\Pi'}) + \frac{r\bar\sigma}{g}(\overline{\sigma'u'\Pi'})$$
$$- \frac{r}{g}(\overline{\sigma'u'})(\overline{\sigma'\Pi'}). \quad$$

Comparing the right-hand side of (6) to (4) relates the eddy PV flux to the E–P flux divergence:

$$-\frac{r\bar\sigma^2}{g}\langle u^*\Pi^*\rangle = \nabla \cdot \mathbf{F} - (r\overline{\sigma'v'})_t - (r\overline{(\sigma\dot\theta)'v'})_\theta$$
$$+ r\bar\sigma\overline{\dot\theta^* v_\theta} - r\overline{(\sigma u)'f'} + r\overline{\sigma'F^{\lambda'}}. \quad (A7)$$

For adiabatic frictionless motion on an f-plane, (7) reduces to

$$-\frac{r\bar\sigma^2}{g}\langle u^*\Pi^*\rangle = \nabla \cdot \mathbf{F} - (r\overline{\sigma'v'})_t, \quad (A8)$$

which states that the eddy PV flux is equal to the pseudo E–P flux divergence (Tung 1986).

In the body of the paper the effects of eddy activity on the local time change of the mean tangential wind are examined. Substitution of (2) into (5) produces the following identity:

$$(r\bar\sigma\bar v)_t + r^{-1}(r^2(\overline{\sigma u})\bar v)_r + (r(\overline{\sigma\dot\theta})\bar v)_\theta$$
$$= r\bar\sigma(\bar v)_t + (\overline{\sigma u})(r\bar v)_r + (\overline{\sigma\dot\theta})(r\bar v)_\theta.$$

Use of the above expression to convert the left-hand side of (4) from flux to advective form yields

$$(\bar v)_t + r^{-1}\langle u\rangle(r\bar v)_r + \langle\dot\theta\rangle(\bar v)_\theta + \langle u\rangle\bar f$$
$$= (r\bar\sigma)^{-1}\nabla \cdot \mathbf{F} - \bar\sigma^{-1}(\overline{(\sigma\dot\theta)'v'})_\theta$$
$$- \bar\sigma^{-1}(\overline{\sigma'v'})_t - \bar\sigma^{-1}\overline{(\sigma u)'f'} + \langle\sigma F^\lambda\rangle$$
$$= -\frac{\bar\sigma}{g}\langle u^*\Pi^*\rangle - (\overline{\dot\theta^* v_\theta}) + \overline{F^\lambda}. \quad (A9)$$

For a steady state ($\bar v_t = (\overline{\sigma'v'})_t = 0$ and $\bar\sigma_t = 0$), it can be seen from (2) that $\overline{\sigma u} = $ constant $= 0$. Under steady conservative conditions (i.e., $\dot\theta = F^\lambda = 0$), the necessary condition for nonacceleration (Charney and Stern 1962) is the vanishing of eddy PV flux, whether or not spatial variations of f are allowed. On an f-plane, the necessary condition can also be expressed as the vanishing of the pseudo E–P flux divergence.

b. Storm-following coordinate

The storm-following coordinate is related to the fixed coordinate by

$$(G)_{t_L} = (G)_t + \mathbf{v}_c \cdot \nabla(G), \qquad (A10)$$

where subscript L denotes that the variable is in reference to the storm-following coordinate and $\mathbf{v}_c$ is the storm motion vector. A scalar quantity can be substituted directly into (10) independent of any orthogonal coordinate system. For a vector quantity in a curvilinear coordinate system, (10) must be applied to the vector and not separately to the vector components. The relative angular momentum equation in the storm-following coordinate derived from (10) using the horizontal wind vector $\mathbf{v}$ for G is

$$(rv_L)_{t_L} + u_L(rv_L)_r + v(rv_L)_\lambda + \dot{\theta}(rv)_\theta$$

$$= -(\Psi)_\lambda - rfu + F^\lambda - r(v_c)_{t_L}. \quad (A11)$$

The equation for mass continuity in the storm-following coordinate is

$$\sigma_{t_L} + r^{-1}(r\sigma u_L)_r + r^{-1}(\sigma v_L)_\lambda + (\sigma\dot{\theta})_\theta = 0. \quad (A12)$$

Following the same procedures as in the previous section, the storm-following coordinate version of the equation of relative angular momentum weighted by pseudodensity in its E–P flux divergence and potential vorticity flux forms is given by

$$(r\bar{\sigma}\bar{v}_L)_{t_L} + r^{-1}(r^2(\overline{\sigma u_L})\bar{v}_L)_r + (r(\overline{\sigma\dot{\theta}})\bar{v})_\theta + (r\overline{\sigma u_L})\bar{f}$$

$$= \nabla \cdot \mathbf{F}_L - (r\overline{(\sigma\dot{\theta})'v'})_\theta - (r\overline{\sigma'v_L'})_{t_L}$$

$$- r\overline{(\sigma u_L)'f'} - r(\overline{\sigma u_c f}) + r\bar{\sigma}F^\lambda - r\overline{\sigma'(v_c)}_{t_L}$$

$$= -\frac{r\bar{\sigma}^2}{g}\langle u_L^*\Pi_L^*\rangle - r\bar{\sigma}(\overline{\dot{\theta}^*v_\theta})$$

$$- r\bar{\sigma}(\overline{u_c f'}) + r\bar{\sigma}\,\overline{F^\lambda}, \quad (A13)$$

where Π_L^* could also be written as Π^* and

$$\mathbf{F}_L \equiv [-r\overline{(\sigma u_L)'v_L'}, \overline{p'\Psi_\lambda'}].$$

For adiabatic frictionless motion on an f-plane, from (13):

$$-\frac{r\bar{\sigma}^2}{g}\langle u_L^*\Pi_L^*\rangle = \nabla \cdot \mathbf{F}_L - (r\overline{\sigma'v_L'})_{t_L}$$

$$- r(\overline{\sigma'u_c'})f_0 - r\overline{\sigma'(v_c)}_{t_L}. \quad (A14)$$

The last two terms arise solely as a result of storm motion and acceleration, respectively.

c. Scaling of the E–P flux vector

The scaling of horizontal and vertical components of the E–P flux vectors in Fig. 3 is analogous to that of Edmon et al. (1980): the radial component is multiplied by the actual length on the diagram that represents 1 m of distance, and the vertical component is multi-

plied by the length on the diagram represented by 1 K of θ. It is possible to further scale the E–P flux vectors so that the "apparent" convergence and divergence of the arrows matches the computed $\nabla \cdot \mathbf{F}$. For example, if $\nabla \cdot \mathbf{F} = 0$,

$$\frac{1}{r}\frac{\partial(rF_r)}{\partial r} + \frac{\partial F_\theta}{\partial\theta} = 0.$$

The above expression can be written

$$\frac{\partial}{\partial r}(rF_r) + \frac{\partial}{\partial\theta}(rF_\theta) = 0.$$

As a result, "visual nondivergence," that is, nondivergence as if the plotted coordinates were Cartesian, could be obtained by multiplying each component of $\mathbf{F}$ by r. This was not done, because the coordinates are not Cartesian, and such a procedure would produce incorrect $\mathbf{F}$ vectors. Instead, we chose to have correct vectors whose actual divergence does not reflect the Cartesian divergence implied by the visual orientation of the vectors.

REFERENCES

Bosart, L. F., and J. A. Bartlo, 1991: Tropical storm formation in a baroclinic environment. *Mon. Wea. Rev.*, **119**, 1979–2013.

Charney, J. G., and M. E. Stern, 1962: On the stability of internal baroclinic jets in a rotating atmosphere. *J. Atmos. Sci.*, **19**, 159–172.

Davis, C. A., 1992: Piecewise potential vorticity inversion. *J. Atmos. Sci.*, **49**, 1397–1411.

——, and K. A. Emanuel, 1991: Potential vorticity diagnostics of cyclogenesis. *Mon. Wea. Rev.*, **119**, 1929–1953.

DeMaria, M., and J. Kaplan, 1994: A statistical hurricane intensity prediction scheme (SHIPS) for the Atlantic Basin. *Wea. Forecasting*, **9**, 209–220.

——, J.-J. Baik, and J. Kaplan, 1993: Upper-level eddy angular momentum fluxes and tropical cyclone intensity change. *J. Atmos. Sci.*, **50**, 1133–1147.

Edmon, H. J., B. J. Hoskins, and M. E. McIntyre, 1980: Eliassen-Palm cross sections for the troposphere. *J. Atmos. Sci.*, **37**, 2600–2616; 1981:Corrigendum, **38**, 1115 p.

Elsberry, R. L., and P. J. Kirchoffer, 1988: Upper-level forcing of explosive cyclogenesis over the ocean based on operationally analyzed fields. *Wea. Forecasting*, **3**, 205–216.

Emanuel, K. A., 1986: An air–sea interaction theory for tropical cyclones. Part I: Steady-state maintenance. *J. Atmos. Sci.*, **43**, 585–604.

——, J. D. Neelin, and C. S. Bretherton, 1994: On large-scale circulations in convecting atmospheres. *Quart. J. Roy. Meteor. Soc.*, **120**, 1111–1144.

Farrell, B., 1985: Transient growth of damped baroclinic waves. *J. Atmos. Sci.*, **42**, 2718–2727.

Gray, W. M., 1968: Global view of the origin of tropical disturbances and storms. *Mon. Wea. Rev.*, **96**, 669–700.

Guinn, T. A., and W. H. Schubert, 1993: Hurricane spiral bands. *J. Atmos. Sci.*, **50**, 3380–3403.

Haynes, P. H., 1988: Forced, dissipative generalizations of finite-amplitude wave activity conservation relations for zonal and nonzonal basic flows. *J. Atmos. Sci.*, **45**, 2352–2362.

Holland, G. J., 1983: Angular momentum transports in tropical cyclones. *Quart. J. Roy. Meteor. Soc.*, **109**, 187–210.

Hoskins, B. J., 1990: Theory of extratropical cyclones. *The Erik Palmén Memorial Volume*, Newton and Holopainen, Eds., Amer. Meteor. Soc., 64–80.

——, M. E. McIntyre, and A. W. Robertson, 1985: On the use and significance of isentropic potential vorticity maps. *Quart. J. Roy. Meteor. Soc.,* **111,** 877–946.

McIntyre, M. E., 1993: Isentropic distributions of potential vorticity and their relevance to tropical cyclone dynamics. *Tropical Cyclone Disasters,* Lighthill, G. Holland, Zhemin, and K. Emanuel, Eds., Peking University Press, 143–156.

——, and T. N. Palmer, 1984: The 'surf zone' in the stratosphere. *J. Atmos. Terr. Phys.,* **46,** 825–850.

Molinari, J., and D. Vollaro, 1989a: External influences on hurricane intensity. Part I: Outflow-layer eddy angular momentum fluxes. *J. Atmos. Sci.,* **46,** 1093–1105.

——, and ——, 1989b: Interaction of a hurricane with a baroclinic wave. Preprints, *18th Conf. on Hurricanes and Tropical Meteorology,* San Diego, CA, Amer. Meteor. Soc., 50–51.

——, and ——, 1990: External influences on hurricane intensity. Part II: Vertical structure and response of the hurricane vortex. *J. Atmos. Sci.,* **47,** 1902–1918.

——, ——, and F. Robasky, 1992: Use of ECMWF operational analyses for studies of the tropical cyclone environment. *Meteor. Atmos. Phys.,* **47,** 127–144.

——, ——, and S. Skubis, 1993: Application of the Eliassen balanced model to real-data tropical cyclones. *Mon. Wea. Rev.,* **121,** 2409–2419.

Möller, J. D., and R. K. Smith, 1994: The development of potential vorticity in a hurricane-like vortex. *Quart. J. Roy. Meteor. Soc.,* **120,** 1255–1266.

Montgomery, M. T., and B. F. Farrell, 1993: Tropical cyclone formation. *J. Atmos. Sci.,* **50,** 285–310.

Ooyama, K. V., 1987: Numerical experiments of steady and transient jets with a simple model of the hurricane outflow layer. Preprints, Volume, *17th Conf. on Tropical Meteorology,* Miami, FL, Amer. Meteor. Soc., 318–320.

Plumb, R. A., 1983: A new look at the energy cycle. *J. Atmos. Sci.,* **40,** 1669–1688.

Raymond, D. J., 1992: Nonlinear balance and potential vorticity thinking at large Rossby number. *Quart. J. Roy. Meteor. Soc.,* **118,** 987–1016.

Reilly, D. H., and K. A. Emanuel, 1991: Evidence of upper tropospheric triggering of tropical cyclogenesis. Preprints, *19th Conf. on Hurricanes and Tropical Meteorology,* Miami, FL, Amer. Meteor. Soc., 202–205.

Riehl, H., 1979: *Climate and Weather in the Tropics.* Academic Press, 611 pp.

Ritchie, E. R., and G. J. Holland, 1993: On the interaction of tropical-cyclone-scale vortices. Part I: Observations. *Quart. J. Roy. Meteor. Soc.,* **119,** 1363–1380.

Rotunno, R., and K. A. Emanuel, 1987: An air–sea interaction theory for tropical cyclones. Part II: Evolutionary study using a nonhydrostatic axisymmetric numerical model. *J. Atmos. Sci.,* **44,** 542–561.

Schubert, W. H., 1985: Wave, mean-flow interactions and hurricane development. Preprints, *16th Conf. on Hurricanes and Tropical Meteorology,* Houston, TX, Amer. Meteor. Soc., 140–141.

——, and B. T. Alworth, 1987: Evolution of potential vorticity in tropical cyclones. *Quart. J. Roy. Meteor. Soc.,* **113,** 147–162.

Shapiro, L. J., 1992: Hurricane vortex motion and evolution in a three-layer model. *J. Atmos. Sci.,* **49,** 140–153.

——, and J. L. Franklin, 1995: Potential vorticity in Hurricane Gloria. *Mon. Wea. Rev.,* **123,** 1465–1475.

——, and H. E. Willoughby, 1982: The response of balanced hurricanes to local sources of heat and momentum. *J. Atmos. Sci.,* **39,** 378–394.

Thorncroft, C. D., B. J. Hoskins, and M. E. McIntyre, 1993: Two paradigms of baroclinic-wave life-cycle behaviour. *Quart. J. Roy. Meteor. Soc.,* **119,** 17–55.

Thorpe, A. J., 1985: Diagnosis of balanced vortex structure using potential vorticity. *J. Atmos. Sci.,* **42,** 397–406.

Tung, K. K., 1986: Nongeostrophic theory of zonally averaged circulation. Part I: Formulation. *J. Atmos. Sci.,* **43,** 2600–2618.

Willoughby, H. E., 1990: Temporal changes of the primary circulation in tropical cyclones. *J. Atmos. Sci.,* **47,** 242–264.

——, J. A. Clos, and M. G. Shoreibah, 1982: Concentric eye walls, secondary wind maxima, and the evolution of a hurricane vortex. *J. Atmos. Sci.,* **39,** 395–411.

——, H.-L. Jin, S. J. Lord, and J. M. Piotrowicz, 1984: Hurricane structure and evolution as simulated by an axisymmetric, nonhydrostatic numerical model. *J. Atmos. Sci.,* **41,** 1169–1186.

Wu, C.-C., and K. A. Emanuel, 1993: Interaction of a baroclinic vortex with background shear: Application to hurricane movement. *J. Atmos. Sci.,* **50,** 62–76.

——, and ——, 1994: On hurricane outflow structure. *J. Atmos. Sci.,* **51,** 1995–2003.